Published in final edited form as:

Oncogene. 2015 January 15; 34(3): 346–356. doi:10.1038/onc.2013.563.

Non-hematopoietic PAR-2 is essential for matriptase-driven pre-malignant progression and potentiation of ras-mediated squamous cell carcinogenesis

Katiuchia Uzzun Sales[1,2], **Stine Friis**[1,3], **Joanne E. Konkel**[1], **Sine Godiksen**[1,3,4], **Marcia Hatakeyama**[5,6], **Karina K. Hansen**[1], **Silvia Regina Rogatto**[5,6], **Roman Szabo**[1], **Lotte K. Vogel**[3], **Wanjun Chen**[1], **J. Silvio Gutkind**[1], and **Thomas H. Bugge**[1]

[1]Oral and Pharyngeal Cancer Branch, National Institutes of Health, Bethesda, MD, USA

[2]Clinical Research Core, National Institute of Dental and Craniofacial Research, National Institutes of Health, Bethesda, MD, USA

[3]Department of Cellular and Molecular Medicine, Faculty of Health and Medical Science, University of Copenhagen, Copenhagen, Denmark

[4]Department of Biology, Faculty of Science, University of Copenhagen, Copenhagen, Denmark

[5]Department of Urology, Faculty of Medicine, Sao Paulo State University (UNESP), Botucatu, Sao Paulo, Brazil

[6]AC Camargo Cancer Center, Sao Paulo, Brazil

Abstract

The membrane-anchored serine protease, matriptase, is consistently dysregulated in a range of human carcinomas, and high matriptase activity correlates with poor prognosis. Furthermore, matriptase is unique among tumor-associated proteases in that epithelial stem cell expression of the protease suffices to induce malignant transformation. Here, we use genetic epistasis analysis to identify proteinase-activated receptor (PAR)-2-dependent inflammatory signaling as an essential component of matriptase-mediated oncogenesis. In cell-based assays, matriptase was a potent activator of PAR-2, and PAR-2 activation by matriptase caused robust induction of NFκB through Gαi. Importantly, genetic elimination of PAR-2 from mice completely prevented matriptase-induced pre-malignant progression, including inflammatory cytokine production, inflammatory cell recruitment, epidermal hyperplasia, and dermal fibrosis. Selective ablation of PAR-2 from bone marrow-derived cells did not prevent matriptase-driven pre-malignant progression, indicating that matriptase activates keratinocyte stem cell PAR-2 to elicit its pro-inflammatory and pro-tumorigenic effects. When combined with previous studies, our data suggest that dual induction of PAR-2-NFκB inflammatory signaling and PI3K-Akt-mTor survival/proliferative

Address correspondence to: Thomas H. Bugge, Ph.D., Oral and Pharyngeal Cancer Branch, National Institute of Dental and Craniofacial Research, National Institutes of Health, 30 Convent Drive, Room 211, Bethesda, MD 20892, Phone: (301) 435-1840, Fax: (301) 402-0823, thomas.bugge@nih.gov.

Conflict of Interest

Authors have declared that no competing interests exist.

signaling underlies the transforming potential of matriptase and may contribute to pro-tumorigenic signaling in human epithelial carcinogenesis.

Keywords

epithelial carcinogenesis; inflammation; keratinocyte stem cells; pericellular proteolysis

Introduction

Dysregulated pericellular proteolytic signaling is a major epigenetic driver of the sequential transformation of a normal human epithelial stem cell to a tumor cell (reviewed in (1)). In this regard, a wealth of evidence has coalesced within the past decade to implicate the aberrant expression and activity of the epithelial membrane-anchored serine protease, matriptase, to the genesis and progression of human epithelial cancers. Matriptase is near ubiquitously expressed in the epithelial compartment of both pre-malignant and malignant human tissues, where its activity is derailed in a variety of manners that include overexpression, misexpression, and loss of posttranscriptional regulation by cognate protease inhibitors (2–15), reviewed in (16, 17). For example, during multi-stage squamous cell carcinogenesis, matriptase expression undergoes a remarkable translocation from post-mitotic suprabasal cells to proliferative cells of the basal compartment, including epithelial stem cells with tumorigenic potential (13, 18). Importantly, we have previously shown that mimicking this translocation by mis-expressing matriptase at low levels in the basal keratinocyte compartment suffices to induce malignant transformation and dramatically potentiates carcinogen-induced tumor formation in transgenic mice (19).

Proteinase-activated receptor (PAR)-2 is a G-protein coupled receptor with pleiotropic functions in vertebrate development and in the maintenance of postnatal homeostasis. Dysregulated PAR-2 activation is believed to contribute to a vast number of common human diseases, owed in particular to the ability of the receptor to induce key inflammatory signaling pathways (20–23). PAR-2 was originally identified as a protease activated receptor that was distinct from PAR-1 in that it responded poorly to thrombin, but was efficiently activated by the digestive enzyme trypsin (24). Subsequently, a large number of trypsin-like serine proteases were shown to be able to activate PAR-2 in various cell-based assays. These include coagulation factors FVIIa and FXa, facilitated by FVIIa binding to tissue factor (25–27), mast cell alpha and beta tryptases, kallikreins 4, 5, 6, and 14 (28–30), as well as the membrane-anchored serine proteases, human airway trypsin-like serine protease (31), TMPRSS2 (32), prostasin (21), hepsin (21), and matriptase (33). Despite the profusion of proteases displaying the capacity to activate PAR-2 *ex vivo*, the specific protease or repertoire of proteases that activates the receptor in many physiological and pathological contexts *in vivo* remains to be established.

PAR-2 is expressed by both primary keratinocytes and by established keratinocyte cell lines (34, 35) where its activation can elicit a range of cellular responses. These include inositol phospholipid hydrolysis and calcium mobilization (34), activation of c-Jun N-terminal kinase, p38 mitogen-activated protein kinase and Rho (36, 37), induction of NFκB activity

(37), secretion of inflammatory cytokines, including granulocyte-macrophage colony-stimulating factor (GM-CSF), interleukin-6 (38), interleukin-8/CXCL1/Gro-1 (35), and thymic stromal lymphopoietin (39), as well as release of prostaglandin (PG)E_2 and PGF_{2a} (40), and expression of intercellular cell adhesion molecule-1 (41).

In this study, we determined the specific contribution of PAR-2 to the oncogenic activity of matriptase, because matriptase-induced squamous cell carcinogenesis is preceded by a signature chronic inflammation, and because the protease and the G-protein coupled receptor are co-expressed in normal squamous epithelium and in squamous cell carcinoma (15, 19, 42). We took advantage of the fact that PAR-2 deficiency in mice causes partial embryonic lethality, but that born offspring is healthy and display normal long-term survival, thus enabling the use of a definitive genetic epistasis analysis to address this issue (21, 43). Importantly, we show that both matriptase-driven pre-malignant progression and the potentiation of carcinogen-induced squamous cell carcinogenesis by matriptase are entirely dependent on non-hematopoietic PAR-2. Furthermore, we show that matriptase activation of PAR-2 leads to pro-tumorigenic inflammatory cytokine release via activation of NFκB through Gαi. The study identifies matriptase as a candidate *in vivo* activator of PAR-2 in the context of human tumorigenesis and demonstrates the importance of posttranscriptional deregulation of PAR-2 signaling to epithelial malignant transformation.

Results

Loss of PAR-2 prevents matriptase-induced pre-malignant progression of mouse squamous epithelium

Matriptase is exclusively expressed in the suprabasal compartment of homeostatic mouse epidermis, but the protease becomes expressed in the stem cell compartment upon exposure to tumor-promoting agents (13, 18). Mimicking this translocation of matriptase expression by low-level expression of a mouse matriptase cDNA under the control of a keratin-5 promoter in transgenic mice (hereafter termed *K5-Mat*$^{+/0}$ mice) leads to spontaneous multi-stage squamous cell carcinogenesis with tumor formation beginning at one year of age (19). PAR-2 is expressed in the keratinocyte compartment and has been hypothesized to be an important mediator of skin inflammation following its activation by trypsin-like serine proteases (see Introduction). Therefore, to determine the possible contribution of PAR-2 to matriptase-mediated squamous cell carcinogenesis, we interbred *K5-Mat*$^{+/0}$ mice and PAR-2-deficient (*F2rl1*$^{-/-}$) mice to generate cohorts of *K5-Mat*$^{+/0}$;*F2rl1*$^{-/-}$ and their associated littermate *K5-Mat*$^{+/0}$;*F2rl1*$^{+/+}$, *F2rl1*$^{-/-}$, and wildtype mice. The outward appearance and health of the mice were followed for 52 weeks, after which the mice were sacrificed for histological examination. As reported previously, *K5-Mat*$^{+/0}$ mice at this age presented with alopecia secondary to follicular metaplasia and ichthyosis (Figure 1A, left panel and data not shown), epidermal hyperplasia (Figure 1B) and hyperproliferation (Figure 1C), multifocal dysplasia (Figure 1D, example with arrowhead), and expression of the stress-associated marker, keratin-6 in the interfollicular epidermis (Figure 1H). As also reported previously, dermal fibrosis with increased dermal cellularity was prominent (Figure 1L). Unexpectedly, however, even at this advanced age, *K5-Mat*$^{+/0}$;*F2rl1*$^{-/-}$ mice did not display alopecia (Figure 1A, second panel from left), epidermal hyperplasia (Figure 1B),

epidermal hyperproliferation (Figure 1C), dysplasia (Figure 1E), interfollicular keratin-6 expression (Figure 1I), or dermal fibrosis (Figure 1M) and, in fact, were outwardly and microscopically indistinguishable in all respects from their *F2rl1*$^{-/-}$, and wildtype littermates (Figure 1A, compare second panel from left with third and fourth panel, Figure 1B and C, compare Figure 1E with F and G, I with J and K, and M with N and O). Taken together, these data reveal that matriptase-mediated pre-malignant progression is entirely PAR-2-dependent.

Matriptase fails to potentiate chemical carcinogenesis in the absence of PAR-2

In addition to initiating spontaneous malignant progression, dysregulated matriptase potentiates *ras*-dependent squamous cell carcinogenesis induced by topical application of the carcinogen, 7,12-dimethylbenzanthracene (DMBA) (19). To establish the contribution of PAR-2 to matriptase-mediated potentiation of chemically-induced squamous cell carcinogenesis, we exposed *K5-Mat*$^{+/0}$;*F2rl1*$^{-/-}$ mice and their associated *K5-Mat*$^{+/0}$;*F2rl1*$^{+/-}$, *F2rl1*$^{-/-}$, and *F2rl1*$^{+/-}$ littermates to repeated DMBA applications, and then observed the formation of tumors by outward inspection of mice for up to 63 weeks (Figure 2A, examples of individual mice in C–F). Because *F2rl*$^{+/-}$ mice are phenotypically normal, and because phenotypic differences observed between *F2rl*$^{+/-}$ and *F2rl*$^{-/-}$ mice can be assumed to be identical to or greater than differences observed between *F2rl*$^{+/+}$ and *F2rl*$^{-/-}$ mice, *K5-Mat;F2rl*$^{+/-}$ and *F2rl*$^{+/-}$ mice were used as controls to simplify the complex breeding scheme needed to littermate control the study. As expected, tumor formation was strongly accelerated in *K5-Mat*$^{+/0}$ mice when compared to littermate controls (median tumor-free survival of 25 weeks for *K5-Mat*$^{+/0}$;*F2rl1*$^{+/-}$ versus 48 weeks for *F2rl1*$^{+/-}$; P <0.0001, log-rank test, two-tailed). *K5-Mat*$^{+/0}$ mice also had to be euthanized faster than littermate control mice due to the tumor burden and the tumor morbidity reaching study endpoints (Figure 2B) (median time to euthanization, 41 weeks for *K5-Mat*$^{+/0}$;*F2rl1*$^{+/-}$ versus 62 weeks for *F2rl1*$^{+/-}$, P <0.004, Wilcoxon rank sum test, two-tailed). Dysregulated matriptase, however, failed to accelerate DMBA-induced squamous cell carcinogenesis when PAR-2 was genetically eliminated. Thus, tumor latency (median tumor-free survival of 45 weeks for *K5-Mat*$^{+/0}$;*F2rl1*$^{-/-}$ versus 48 weeks for *F2rl1*$^{-/-}$ and 48 weeks for *F2rl1*$^{+/-}$; P = N.S., Kaplan-Meier log rank test), and time to euthanization (median time to euthanization of 61 weeks for *K5-Mat*$^{+/0}$;*F2rl1*$^{-/-}$ versus 56 weeks for *F2rl1*$^{-/-}$, and 62 weeks for *F2rl1*$^{+/-}$; P = N.S., Wilcoxon rank sum test, two-tailed) was similar to control and to PAR-2-deficient mice (Figure 2A and B). Total tumor burden at euthanization (Figure 2B) and histological appearance of tumors (Figure 2G–N), did not differ between mice of different genotypes, with all mice presenting with squamous cell carcinoma of variable degrees of differentiation.

Non-hematopoietic cell-derived PAR-2 mediates matriptase-driven pre-malignant progression

PAR-2 is expressed not only by keratinocytes, but also by a variety of leukocyte populations that infiltrate the skin during pre-neoplastic progression. We therefore next examined if the failure of PAR-2-deficient mice to promote the stereotypic pro-tumorigenic proliferative responses that are associated with dysregulated epidermal matriptase were caused by loss of keratinocyte matriptase-PAR-2 signaling or, rather, were an indirect consequence of

intrinsic defects of PAR-2-deficient leukocytes. For this purpose, we performed bone marrow chimeric studies in which *K5-Mat*$^{+/0}$ and wildtype littermate mice were lethally irradiated and thereafter reconstituted with histocompatible bone marrow from either *F2rl1*$^{+/+}$ or *F2rl1*$^{-/-}$ mice. Successful bone marrow transplantation was ensured by FACS analysis for expression of donor-specific hematopoietic markers (Supplementary Figure 1). After recovery from grafting, the bone marrow chimeric mice were followed for 11 weeks and then sacrificed and examined (Figure 3). As predicted, *K5-Mat*$^{+/0}$ mice grafted with wildtype bone marrow displayed epidermal hyperplasia, epidermal hyperproliferation, and dermal fibrosis when compared to wildtype mice grafted with wildtype bone marrow (Figure 3A and B, compare example in C with E, and example in G with I). No diminution of hyperplasia, hyperproliferation, and fibrosis was apparent when *K5-Mat*$^{+/0}$ mice were grafted with PAR-2-deficient bone marrow (Figure 3A and B, compare example in D with F, and example in H with J). Thus, epithelial hyperplasia, hyperproliferation and dermal collagen density all were similar in *K5-Mat*$^{+/0}$ mice grafted with either PAR-2-deficient or PAR-2-sufficient bone marrow. These data demonstrate that dysregulated matriptase activates PAR-2 on cells of non-hematopoietic origin to elicit its tumor-promoting effects.

Dysregulated matriptase fails to elicit dermal inflammatory cell recruitment in the absence of PAR-2

Matriptase-induced pre-malignant progression is associated with a signature accumulation of inflammatory cells in the dermis (13, 19). To explore if dysregulated matriptase induces inflammatory cell recruitment through PAR-2, we enumerated dermal mast cells in young (8–10 week old) littermate and older (52-week-old) littermate *K5-Mat*$^{+/0}$;*F2rl1*$^{+/+}$, *K5-Mat*$^{+/0}$;*F2rl1*$^{-/-}$, *F2rl1*$^{+/+}$, and *F2rl1*$^{-/-}$ mice (Figure 4). In both younger (Figure 4A–D, and I) and older (Figure 4E–H, and J) mice, a significant increase in mast cell accumulation was observed in *K5-Mat*$^{+/0}$ mice compared to wildtype littermates. Interestingly, however, elimination of PAR-2 completely negated the matriptase-induced increase in mast cell accumulation, with the number of dermal mast cells in *K5-Mat*$^{+/0}$;*F2rl1*$^{-/-}$ mice being similar to wildtype and *F2rl1*$^{-/-}$ littermates (compare example in Figure 4B with C and D, I, and Figure 4F with G and H, J). This data suggest that dysregulated matriptase mediates inflammatory cell recruitment through PAR-2.

Dysregulated matriptase induces inflammatory cytokine release through PAR-2

We next explored if the dramatic impact of global PAR-2 ablation on matriptase-driven pre-malignant progression could be related to the elimination of a keratinocyte-intrinsic matriptase-PAR-2-mediated inflammatory signaling pathway. For this purpose, we performed qPCR analysis of skin cells to determine the mRNA levels of a number of keratinocyte-produced inflammatory cytokines and inflammatory mediators in young (8 to10-week-old) *K5-Mat*$^{+/0}$;*F2rl1*$^{-/-}$ mice and their associated *K5-Mat*$^{+/0}$;*F2rl1*$^{+/+}$, *F2rl1*$^{-/-}$, and wildtype littermates. These included mRNAs encoding the murine interleukin 8 equivalent, chemokine (C-X-C motif) ligand 1 (*Cxcl1*), interleukin-1β (*Il1b)*, thymic stromal lymphopoietin (*Tslp*), colony stimulating factor 2 (*Csf2*), tumor necrosis factor (*Tnf*), interferon-γ (*Ifn*γ), and intercellular adhesion molecule 1 (*Icam1*) (Figure 5A–G). mRNA levels of *Cxcl1*, *Il1b*, *Tslp*, *Csf2*, *Tnf* and *Icam1* all were significantly increased (2–171 fold) in young *K5-Mat*$^{+/0}$ mice when compared to their wildtype littermates (Figure 5A–E, G),

and *Ifng* mRNA displayed a 3.6 fold increase without reaching statistical significance (Figure 5F). This result demonstrates that dysregulated matriptase induces expression of skin inflammatory mediators. Importantly, loss of PAR-2 from *K5-Mat*$^{+/0}$ mice reduced the level of expression of *Cxcl1*, *Il1b*, *Tslp*, *Csf2*, and *Tnf* mRNA species to levels similar to those observed in wildtype and *F2rl1*$^{-/-}$ mice (Figure 5A–E) suggesting that keratinocyte PAR-2 is required for matriptase-induced expression of these cytokines. To substantiate this hypothesis, we next measured mRNA levels of *Cxcl1*, *Il1b*, *Tslp*, *Csf2*, *Tnf*, *Ifng*, and *Icam1* in 17-week-old *K5-Mat*$^{+/0}$ mice reconstituted with, respectively, PAR-2-deficient and -sufficient bone marrow (Figure 5H–N). As expected, mRNA levels of *Cxcl1*, *Il1b*, *Tslp*, *Tnf*, *Ifng*, and *Icam1* (Figure 5H–J, L–N) all were significantly increased in *K5-Mat*$^{+/0}$ mice reconstituted with wildtype bone marrow when compared to control mice (wildtype mice reconstituted with either wildtype or PAR-2-deficient bone marrow), while *Csf2* mRNA was 1.7-fold increased without reaching statistical significance (Figure 5K). *Il1b*, *Tslp*, *Tnf*, *Ifng*, and *Icam* mRNA levels remained significantly increased in *K5-Mat*$^{+/0}$ mice reconstituted with PAR-2-deficient bone marrow (Figure 5I, J, L, M, and N), while *Cxcl1* and *Csf2* mRNA were, respectively, 1.8 and 1.7-fold increased (Figure 5H and K) without reaching statistical significance, showing that hematopoietic PAR-2 is dispensable for the induction of expression of skin inflammatory mediators by dysregulated matriptase through PAR-2. Analysis of skin from 52-week-old mice showed a significant increase in *Cxcl1*, *Il1b*, *Tslp*, and *Csf2* mRNA levels of *K5-Mat*$^{+/0}$ mice when compared to wildtype littermates (Figure 5O–R). The levels of these four cytokine mRNA species were reduced, 24-, 8-, 35-, and 47–fold, respectively, by PAR-2 elimination, reaching significance for *Cxcl1*, while not reaching significance for *Il1b*, *Tslp*, and *Csf2* ($p < 0.13$, 0.065, and 0.070, respectively). Taken together, the data indicate that dysregulated matriptase induces early expression of key pro-tumorigenic inflammatory mediators through keratinocyte PAR-2.

Matriptase activates NFκB through PAR-2 and Gαi

Because NFκB is a key epidermal regulator of inflammatory cytokine production in both non-neoplastic and neoplastic contexts (44, 45) and because many of the cytokines whose mRNAs were increased in *K5-Mat*$^{+/0}$ mice are regulated by NFκB, we investigated if matriptase activation of PAR-2 could induce NFκB activity in epithelial cells. For this purpose, we used a recently established reconstituted cell-based assay (46, 47) in which HEK293 cells were transfected with a PAR-2 expression vector and either a serum response element-luciferase reporter plasmid or NFκB-luciferase reporter plasmid. The transfected cells then were exposed to either a PAR-2 agonist, a dual PAR-1 and PAR-2 agonist or to soluble recombinant matriptase. As described recently (47), a dose-dependent increase in serum response element activity was observed when PAR-2-transfected cells were exposed to a PAR-2 agonist peptide (Figure 6A, bars 1–5) or the dual PAR-1 and -2 agonist peptide (Figure 6A, bar 6). A similar dose-dependent increase in serum response element activity was observed when PAR-2 transfected cells (Figure 6B, bars 1–3) but not mock transfected cells (Figure 6B, bar 4) were exposed to matriptase. Importantly, exposure of PAR-2 transfected cells to the PAR-2 agonist peptide (Figure 6C, bars 1–5), the dual PAR-1 and -2 agonist peptide (Figure 6C, bar 6) or to matriptase (Figure 6D, bar 1–3) also elicited dose-dependent NFκB activity. When PAR-2 was substituted with PAR-1, the dual PAR-1 and -2 agonist (Figure 6E, bar 1–5), but not the PAR-2 agonist (Figure 6E, bar 6) or soluble

recombinant matriptase (Figure 6F, bar 1–3, compare with bar 4) induced a dose-dependent increase in serum response element activity, showing that soluble recombinant matriptase selectively activates PAR-2. Although PAR-1 induced serum response element activity in response to the dual PAR-1 and -2 agonist (Figure 6E, bars 1–5, compare to bar 6), the activated receptor failed to induce NFκB activity (Figure 6G, bars 1–5, compare to bar 6) or, as expected, when exposed to soluble recombinant matriptase (Figure 6H, bar 1–3, compare with bar 4). To further explore this matriptase-PAR-2-NFκB signaling pathway, we next attempted to identify the G protein that couples to matriptase-activated PAR-2 to elicit NFκB activation. Co-introduction of dominant-negative RGS-βARK (Figure S3A, B, E and G) and PDZrhoGEF (Figure S3C, D, F and H) mutants that target, respectively, Gαq/11 and Gα12/13, to the PAR-2 expression vector- and NFκB reporter plasmid-transfected cells did not affect the induction of NFκB activity by either the PAR-2 agonist or by recombinant soluble matriptase. To specifically determine the involvement of Gαi, HEK293 cells were mock transfected (Figure 6I, bar 1 and 2) or transfected with the PAR-2 expression vector and the NFκB reporter plasmid were either untreated (Figure 6I, bar 3 and 4) or exposed to PAR-2 agonist (Figure 6I, bars 5 and 6) or soluble recombinant matriptase (Figure 6I, bars 7 and 8) and treated with either vehicle (Figure 6I, bars 1, 3, 5, and 7) or pertussis toxin (PTX, Figure 6I, bars 2, 4, 6, and 8). As observed in Figure 6C and D), both the PAR-2 agonist and matriptase induced NFκB activity (Figure 6I, compare bar 3 with bars 5 and 7). Pertussis toxin strongly reduced both PAR-2 agonist (Figure 6I, compare bar 5 with bar 6) and matriptase-induced (Figure 6I, compare bar 7 with bar 8) NFκB activity. Interestingly, using the identical experimental setup, pertussis toxin had only a minor effect on the ability of activated PAR-2 to induce serum response element activity (Figure 6J). Taken together, these data demonstrate that matriptase-activated PAR-2 selectively signals through Gαi to activate NFκB.

We recently identified pro-HGF activation as a critical mechanism by which dysregulated matriptase promotes squamous cell carcinogenesis, based on the failure of matriptase to accelerate tumor progression in mice with specific ablation of the HGF receptor, c-Met, from the keratinocyte stem cell compartment (13). Interestingly, however, unlike PAR-2 ablation, loss of c-Met failed to prevent mast cell accumulation in response to dysregulated matriptase, with the number of mast cells being similar in c-Met-sufficient *K5-Mat*$^{+/0}$ and c-Met-deficient *K5-Mat*$^{+/0}$ mice (Supplementary Figure 3A–D). Furthermore, activation of PAR-2, by targeting cells with soluble recombinant matriptase for up to 3 h failed to induce transactivation of c-Met, as evidenced by the absence of autophosphorylation of c-Met and phosphorylation of Gab-1 (Supplementary Figure 3E and F). These data indicate that activation of PAR-2 and c-Met by matriptase induces separate pro-tumorigenic signaling pathways and that each is required for the promotion of squamous cell carcinogenesis by the membrane-anchored serine protease.

Discussion

Multiple studies have linked dysregulated matriptase to human epithelial carcinogenesis, but the molecular mechanisms by which the membrane protease promotes carcinogenesis are only beginning to be elucidated. Here we employed genetic epistasis analysis to specifically query the contribution of one candidate substrate, PAR-2, to matriptase-driven squamous

cell carcinogenesis. Unexpectedly, we found that genetically eliminating PAR-2 sufficed to negate all pro-tumorigenic effects of dysregulated epidermal matriptase. Thus, matriptase-driven pre-malignant progression did not occur in the absence of PAR-2, and dysregulated matriptase failed to potentiate DMBA-induced carcinogenesis in the absence of the G-protein coupled receptor. Specific ablation of PAR-2 from hematopoietic cells did not affect matriptase-mediated pre-malignant progression, suggesting that dysregulated matriptase activates epidermal (most likely keratinocyte) PAR-2 to promote malignant progression. Because matriptase and PAR-2 has been shown to be consistently co-expressed in the epithelial compartment of human squamous cell carcinoma (15), the current study provides strong evidence that a matriptase-PAR-2 signaling axis contributes to human squamous cell carcinogenesis.

We have previously shown that matriptase-driven squamous cell carcinogenesis is preceded by a conspicuous recruitment of large numbers of mast cells to the underlying dermis (19). The current study provides evidence that this effect of matriptase dysregulation is related to PAR-2-dependent NFκB activation via Gαi and the associated release of NFκB-dependent inflammatory cytokines. Firstly, the matriptase-mediated increase in the mRNA levels of several NFκB-induced inflammatory cytokines was entirely dependent on non-hematopoietic PAR-2. Secondly, in a reconstituted cell-based system, matriptase activation of PAR-2 induced a robust activation of an NFκB reporter gene via Gαi. Because the causal association between chronic inflammation and epithelial carcinogenesis is well established, it is possible that the elicitation of pro-inflammatory cytokines via NFκB activation could account for all the pro-tumorigenic effects associated with untimely activation of PAR-2 by matriptase. The current study, however, does not exclude other PAR-2 activation-induced effects, such as the direct stimulation of proliferation, cell death protection or motility enhancement. Our findings are aligned with a previous study showing that soluble matriptase can induce cytokine release in cultured human endothelial cells through PAR-2 and NFκB (48).

By using a genetic epistasis approach similar to the current study, we have previously shown that dysregulated matriptase promotes squamous cell carcinogenesis by activating a c-Met-Akt-signaling pathway by proteolytic conversion of pro-HGF to active HGF on the keratinocyte cell surface (13). Interestingly, in this study, imposition of either PAR-2 or c-Met deficiency on *K5-Mat*$^{+/0}$ transgenic mice negated the ability of dysregulated matriptase to potentiate DMBA-induced tumorigenesis and blocked matriptase-driven pre-malignant progression, including epidermal hyperproliferation, dysplasia, follicular metaplasia, expression of stress-associated epidermal keratins, and induction of dermal fibrosis. Analysis of archived tissues from c-Met-sufficient *K5-Mat*$^{+/0}$ and c-Met-deficient *K5-Mat*$^{+/0}$ mice did, however, reveal that loss of c-Met signaling, unlike loss of PAR-2 signaling, failed to prevent matriptase-induced inflammatory cell recruitment. Furthermore, although PAR-2 has been proposed to transactivate c-Met in the context of hepatocellular carcinoma invasion (49), we found no evidence that PAR-2 activation was associated with increased c-Met activity using a reconstituted cell-based assay using HEK cells or using immortalized keratinocytes. An intriguing unanswered question that arises from these studies, therefore, is why matriptase-induced inflammatory PAR-2 signaling does not

promote malignant progression in the absence of activated c-Met and, conversely, why matriptase-induced c-Met-Akt signaling does not promote malignant progression in the absence of activated PAR-2.

In summary, by performing genetic epistasis analysis in an animal model, in which the signature dysregulation of matriptase in human carcinomas is mimicked by low level mis-expression of matriptase in the epidermis (19), we have provided definitive evidence that matriptase proteolytically cleaves both PAR-2 and pro-HGF *in vivo* to activate, respectively, tumor promoting G-protein coupled and receptor tyrosine kinase signaling pathways. Furthermore, we have shown that both pathways must be activated simultaneously by matriptase for the protease to exert its tumor promoting effects on squamous epithelium. The study underscores that pericellular serine proteases may be excellent therapeutic targets for the prevention and treatment of cancer, due to their convenient extracellular location and their capacity to regulate fundamental pro-tumorigenic cellular signaling pathways.

Materials and Methods

Animals

All experiments were performed in an Association for Assessment and Accreditation of Laboratory Animal Care International-accredited vivarium following Institutional Guidelines and standard operating procedures. The generation of mice overexpressing matriptase under the keratin-5 promoter (*K5-Mat*$^{+/0}$) has been reported previously (19). Mice carrying a *F2rl1* null allele (50) were purchased from the Jackson Laboratories (Bar Harbor, ME). *K5-Mat*$^{+/0}$; *F2rl1*$^{-/-}$ and *K5-Mat*$^{+/0}$;*F2rl1*$^{+/+}$, *K5-Mat*$^{+/0}$; *F2rl1*$^{+/-}$, *F2rl1*$^{+/+}$, *F2rl1*$^{+/-}$ and *F2rl1*$^{-/-}$ mice in a mixed (FVB/NJ/C57BL/6J/Black Swiss) background were generated by interbreeding. The study was strictly littermate controlled to avoid genetic background differences from confounding data interpretation.

Chemical carcinogenesis

DMBA was diluted to a final concentration of 250 μg/ml in acetone and 100 μl was applied to the dorsal skin of the mice every three weeks.

Bone marrow chimeras

Bone marrow was isolated from either C57BL/6J-*F2rl1*$^{+/+}$ mice or from C57BL/6J-*F2rl1*$^{-/-}$ mice and was injected intravenously into lethally irradiated (900 rads) six-week-old *K5-Mat*$^{+/0}$ and wild-type littermate control F1 offspring from FVB/NJ-*K5-Mat*$^{+/0}$ mice crossed to C57BL/6J mice. DMBA treatment was performed 8 weeks after transplantation as described above.

Histological and immunohistochemical analysis

Skin and tumor tissues were fixed for 24 h in 4% paraformaldehyde (PFA) in phosphate buffered saline (PBS), processed into paraffin, sectioned into sagittal 3-μm sections and stained with hematoxylin and eosin, Masson's trichrome or toluidine blue prior to histopathological assessment. Immunohistochemical analysis was performed as described previously (51). Antibodies recognizing keratin-6 (Covance, Chantilly, VA), and F4/80

(AbD Serotec, Raleigh, NC) were used for staining. Epithelial cell proliferation was visualized by intraperitoneal injection of 10 μg/g of 5-bromo-2′-deoxyuridine (BrdU), 2 h prior to euthanasia. BrdU incorporation was detected with a mouse anti-BrdU antibody (Accurate, Westbury, NY). Bound antibodies were visualized with the Vectastain ABC peroxidase kit as recommended by the manufacturer (Vector Laboratories, Burlingame, CA) and developed with the addition of the 3,3'-diaminobenzidine substrate (Sigma, St Louis, MO). Slides were digitalized using a ScanScope (Aperio, Vista, CA) and the height of the epidermis (epithelial thickness), mast cell count per 10^5 μm^2 and the number of BrdU positive basal cells (basal proliferation rates) were quantified.

RNA preparation and real-time PCR

Whole skin was snap-frozen in liquid nitrogen and ground to a fine powder with mortar and pestle. Total RNA was prepared by extraction in Trizol reagent (Life Technologies, Frederick, MD) as recommended by the manufacturer. Reverse transcription and PCR amplification were performed using the RETROscript™ Kit (Ambion, Inc., Austin, TX), as recommended by the manufacturer. First strand cDNA synthesis was performed using an Oligo dT primer. The following primer pairs were used for qPCR: *Tnf*; 5'-CAGCCTCTTCTCATTCCTGC-3' and 5'- AGGGTCTGGGCCATAGAACT-3'. *Ifng*; 5'-AGCGGCTGACTGAACTCAGATTGTAG-3' and 5'-GTCACAGTTTTCAGCTGTATAGGG-3'. *Il1b*; 5'-GGGCCTCAAAGGAAAGAATC-3' and 5'-TACCAGTTGGGGAACTCTGC-3'. *Gapdh*; 5'-GTGAAGCAGGCATCTGAGG-3' and 5'-CATCGAAGGTGGAAGAGTGG-3'. Annealing temperature for these primer sets was 55°C. Expression levels were normalized to *Gapdh* in each sample. *Tslp, Cxcl1, Icam1* and *Csf2* qPCRs were done using TaqMan probes following the manufacturer's instructions (Life Technologies).

PAR-2 activation assay

The assay was performed as described before (46). Briefly, HEK293 cells were plated on poly-L-lysine-coated 24-well plates and grown in Dulbecco's Modified Eagle Medium (DMEM) (Life Technologies, Frederick, MD) supplemented with 10% fetal bovine serum (FBS) for 24 h. Cells were co-transfected either with pSRE-firefly luciferase (50 ng) (Stratagene, Cedar Creek, TX) or NFκB-firefly luciferase (50 ng) reporter (Stratagene, La Jolla, CA), combined with pRL-Renilla luciferase (20 ng), pcDNA 3.1-PAR-2 (50 ng) or pcDNA 3.1-PAR-1 (50 ng) (Missouri S&T cDNA Resource Center, Rolla, MO) using Lipofectamine according to the manufacturer's instructions (Life Technologies). The medium was changed after 12 h, and 36 h after transfection, the cells were serum-starved overnight and then stimulated with either matriptase (R&D, Minneapolis, MN), PAR-2 agonist peptide ([3H]2-furoyl-LIGRL-NH2) (Tocris, Minneapolis, MN), PAR-1 and-2 agonist peptide (tcY-NH2) (Tocris), or vehicle for 6 h. Cells were washed twice in PBS and luciferase activity was determined using the dual luciferase assay kit (Promega, Madison, WI) according to the manufacturer's instructions. Luminescence was measured using a Microtiter Plate Luminometer (Dynex Technologies, Chantilly, VA) and the SRE activation was determined as the ratio of firefly to Renilla luciferase counts.

G-protein assay

HEK293T cells were plated in 24 well plates and transfected with either SRE-luciferase or NFkB-luciferase reporter together with pRL-Renilla and PAR-2. 36 h post-transfection the cells were serum starved ON with pertussis toxin (50 ng/ml) or with vehicle added to the media in a final concentration. For all three above mentioned G-protein experiments, the cells were stimulated with 10 uM PAR-2 agonist or 15 nM recombinant human matriptase for 6h at 37°C before the luciferase activity was determined.

Supplementary Material

Refer to Web version on PubMed Central for supplementary material.

Acknowledgments

We thank Dr. Mary Jo Danton for critically reviewing this manuscript. Histology was performed by Histoserv, Inc., Germantown, MD. We thank Drs. Allessia Gallo, Shyh-Ing Jang, Colleen Doci, Patricia Pilla, Zhiyong Wang, Canstantinos Mikelis, Ramiro Iglesias-Bartolome, and Morgan O'Hare for technical assistance. The study was supported by the NIDCR Intramural Research Program (THB, JSG, WC), The Augustinus Foundation, Købmand Kristian Kjær og hustrus Foundation, the Kjær-Foundation, the Dagmar Marshalls Foundation, the Snedkermester Sophus Jacobsen og Hustru Astrid Jacobsens Foundation, the Grosserer Valdemar Foersom og Hustru Thyra Foersoms Foundation, and Fabrikant Einar Willumsens Mindelegat (SG and LKV), The Sao Paulo Research Foundation (FAPESP) (MH, SRR).

References

1. Lopez-Otin C, Hunter T. The regulatory crosstalk between kinases and proteases in cancer. Nat Rev Cancer. 2010; 10(4):278–292. [PubMed: 20300104]
2. Benaud C, Oberst M, Hobson JP, Spiegel S, Dickson RB, Lin CY. Sphingosine 1-phosphate, present in serum-derived lipoproteins, activates matriptase. J Biol Chem. 2002; 277(12):10539–10546. [PubMed: 11792696]
3. Hoang CD, D'Cunha J, Kratzke MG, Casmey CE, Frizelle SP, Maddaus MA, et al. Gene expression profiling identifies matriptase overexpression in malignant mesothelioma. Chest. 2004; 125(5): 1843–1852. [PubMed: 15136399]
4. Jin JS, Chen A, Hsieh DS, Yao CW, Cheng MF, Lin YF. Expression of serine protease matriptase in renal cell carcinoma: correlation of tissue microarray immunohistochemical expression analysis results with clinicopathological parameters. Int J Surg Pathol. 2006; 14(1):65–72. [PubMed: 16501837]
5. Jin JS, Hsieh DS, Loh SH, Chen A, Yao CW, Yen CY. Increasing expression of serine protease matriptase in ovarian tumors: tissue microarray analysis of immunostaining score with clinicopathological parameters. Mod Pathol. 2006; 19(3):447–452. [PubMed: 16439987]
6. Johnson MD, Oberst MD, Lin CY, Dickson RB. Possible role of matriptase in the diagnosis of ovarian cancer. Expert Rev Mol Diagn. 2003; 3(3):331–338. [PubMed: 12779007]
7. Kang JY, Dolled-Filhart M, Ocal IT, Singh B, Lin CY, Dickson RB, et al. Tissue microarray analysis of hepatocyte growth factor/Met pathway components reveals a role for Met, matriptase, and hepatocyte growth factor activator inhibitor 1 in the progression of node-negative breast cancer. Cancer Res. 2003; 63(5):1101–1105. [PubMed: 12615728]
8. Lee JW, Yong Song S, Choi JJ, Lee SJ, Kim BG, Park CS, et al. Increased expression of matriptase is associated with histopathologic grades of cervical neoplasia. Hum Pathol. 2005; 36(6):626–633. [PubMed: 16021568]
9. Oberst M, Anders J, Xie B, Singh B, Ossandon M, Johnson M, et al. Matriptase and HAI-1 are expressed by normal and malignant epithelial cells in vitro and in vivo. Am J Pathol. 2001; 158(4): 1301–1311. [PubMed: 11290548]

10. Oberst MD, Johnson MD, Dickson RB, Lin CY, Singh B, Stewart M, et al. Expression of the serine protease matriptase and its inhibitor HAI-1 in epithelial ovarian cancer: correlation with clinical outcome and tumor clinicopathological parameters. Clin Cancer Res. 2002; 8(4):1101–1107. [PubMed: 11948120]
11. Tanimoto H, Shigemasa K, Tian X, Gu L, Beard JB, Sawasaki T, et al. Transmembrane serine protease TADG-15 (ST14/Matriptase/MT-SP1): expression and prognostic value in ovarian cancer. Br J Cancer. 2005; 92(2):278–283. [PubMed: 15611789]
12. Vogel LK, Saebo M, Skjelbred CF, Abell K, Pedersen ED, Vogel U, et al. The ratio of Matriptase/HAI-1 mRNA is higher in colorectal cancer adenomas and carcinomas than corresponding tissue from control individuals. BMC cancer. 2006; 6:176. [PubMed: 16820046]
13. Szabo R, Rasmussen AL, Moyer AB, Kosa P, Schafer J, Molinolo A, et al. c-Met-induced epithelial carcinogenesis is initiated by the serine protease matriptase. Oncogene. 2011; 30:2003–2016. [PubMed: 21217780]
14. Lebeau AM, Lee M, Murphy ST, Hann BC, Warren RS, Delos Santos R, et al. Imaging a functional tumorigenic biomarker in the transformed epithelium. Proc Natl Acad Sci U S A. 2013; 110(1):93–98. [PubMed: 23248318]
15. Bocheva G, Rattenholl A, Kempkes C, Goerge T, Lin CY, D'Andrea MR, et al. Role of matriptase and proteinase-activated receptor-2 in nonmelanoma skin cancer. J Invest Dermatol. 2009; 129(7):1816–1823. [PubMed: 19242518]
16. List K. Matriptase: a culprit in cancer? Future Oncol. 2009; 5(1):97–104. [PubMed: 19243302]
17. Bugge TH, Antalis TM, Wu Q. Type II transmembrane serine proteases. J Biol Chem. 2009; 284(35):23177–23181. [PubMed: 19487698]
18. List K, Szabo R, Molinolo A, Nielsen BS, Bugge TH. Delineation of matriptase protein expression by enzymatic gene trapping suggests diverging roles in barrier function, hair formation, and squamous cell carcinogenesis. Am J Pathol. 2006; 168(5):1513–1525. [PubMed: 16651618]
19. List K, Szabo R, Molinolo A, Sriuranpong V, Redeye V, Murdock T, et al. Deregulated matriptase causes ras-independent multistage carcinogenesis and promotes ras-mediated malignant transformation. Genes Dev. 2005; 19(16):1934–1950. [PubMed: 16103220]
20. Schaffner F, Ruf W. Tissue factor and protease-activated receptor signaling in cancer. Semin Thromb Hemost. 2008; 34(2):147–153. [PubMed: 18645919]
21. Camerer E, Barker A, Duong DN, Ganesan R, Kataoka H, Cornelissen I, et al. Local protease signaling contributes to neural tube closure in the mouse embryo. Dev Cell. 2010; 18(1):25–38. [PubMed: 20152175]
22. Coughlin SR, Camerer E. PARticipation in inflammation. J Clin Invest. 2003; 111(1):25–27. [PubMed: 12511583]
23. Rothmeier AS, Ruf W. Protease-activated receptor 2 signaling in inflammation. Semin Immunopathol. 34(1):133–149. [PubMed: 21971685]
24. Nystedt S, Emilsson K, Wahlestedt C, Sundelin J. Molecular cloning of a potential proteinase activated receptor. Proc Natl Acad Sci U S A. 1994; 91(20):9208–9212. [PubMed: 7937743]
25. Camerer E, Huang W, Coughlin SR. Tissue factor- and factor X-dependent activation of protease-activated receptor 2 by factor VIIa. Proc Natl Acad Sci U S A. 2000; 97(10):5255–5260. [PubMed: 10805786]
26. Camerer E, Rottingen JA, Iversen JG, Prydz H. Coagulation factors VII and X induce Ca2+ oscillations in Madin-Darby canine kidney cells only when proteolytically active. J Biol Chem. 1996; 271(46):29034–29042. [PubMed: 8910556]
27. Camerer E, Kataoka H, Kahn M, Lease K, Coughlin SR. Genetic evidence that protease-activated receptors mediate factor Xa signaling in endothelial cells. J Biol Chem. 2002; 277(18):16081–16087. [PubMed: 11850418]
28. Molino M, Barnathan ES, Numerof R, Clark J, Dreyer M, Cumashi A, et al. Interactions of mast cell tryptase with thrombin receptors and PAR-2. J Biol Chem. 1997; 272(7):4043–4049. [PubMed: 9020112]
29. Oikonomopoulou K, Hansen KK, Saifeddine M, Tea I, Blaber M, Blaber SI, et al. Proteinase-activated receptors, targets for kallikrein signaling. J Biol Chem. 2006; 281(43):32095–32112. [PubMed: 16885167]

30. Ramsay AJ, Dong Y, Hunt ML, Linn M, Samaratunga H, Clements JA, et al. Kallikrein-related peptidase 4 (KLK4) initiates intracellular signaling via protease-activated receptors (PARs). KLK4 and PAR-2 are co-expressed during prostate cancer progression. J Biol Chem. 2008; 283(18): 12293–12304. [PubMed: 18308730]
31. Chokki M, Yamamura S, Eguchi H, Masegi T, Horiuchi H, Tanabe H, et al. Human airway trypsin-like protease increases mucin gene expression in airway epithelial cells. Am J Respir Cell Mol Biol. 2004; 30(4):470–478. [PubMed: 14500256]
32. Wilson S, Greer B, Hooper J, Zijlstra A, Walker B, Quigley J, et al. The membrane-anchored serine protease, TMPRSS2, activates PAR-2 in prostate cancer cells. Biochem J. 2005; 388(Pt 3): 967–972. [PubMed: 15537383]
33. Takeuchi T, Harris JL, Huang W, Yan KW, Coughlin SR, Craik CS. Cellular localization of membrane-type serine protease 1 and identification of protease-activated receptor-2 and single-chain urokinase-type plasminogen activator as substrates. J Biol Chem. 2000; 275(34):26333–26342. [PubMed: 10831593]
34. Santulli RJ, Derian CK, Darrow AL, Tomko KA, Eckardt AJ, Seiberg M, et al. Evidence for the presence of a protease-activated receptor distinct from the thrombin receptor in human keratinocytes. Proc Natl Acad Sci U S A. 1995; 92(20):9151–9155. [PubMed: 7568091]
35. Hou L, Kapas S, Cruchley AT, Macey MG, Harriott P, Chinni C, et al. Immunolocalization of protease-activated receptor-2 in skin: receptor activation stimulates interleukin-8 secretion by keratinocytes in vitro. Immunology. 1998; 94(3):356–362. [PubMed: 9767417]
36. Scott G, Leopardi S, Parker L, Babiarz L, Seiberg M, Han R. The proteinase-activated receptor-2 mediates phagocytosis in a Rho-dependent manner in human keratinocytes. J Invest Dermatol. 2003; 121(3):529–541. [PubMed: 12925212]
37. Kanke T, Macfarlane SR, Seatter MJ, Davenport E, Paul A, McKenzie RC, et al. Proteinase-activated receptor-2-mediated activation of stress-activated protein kinases and inhibitory kappa B kinases in NCTC 2544 keratinocytes. J Biol Chem. 2001; 276(34):31657–31666. [PubMed: 11413129]
38. Wakita H, Furukawa F, Takigawa M. Thrombin and trypsin induce granulocyte-macrophage colony-stimulating factor and interleukin-6 gene expression in cultured normal human keratinocytes. Proc Assoc Am Physicians. 1997; 109(2):190–207. [PubMed: 9069588]
39. Briot A, Deraison C, Lacroix M, Bonnart C, Robin A, Besson C, et al. Kallikrein 5 induces atopic dermatitis-like lesions through PAR2-mediated thymic stromal lymphopoietin expression in Netherton syndrome. J Exp Med. 2009; 206(5):1135–1147. [PubMed: 19414552]
40. Scott G, Leopardi S, Printup S, Malhi N, Seiberg M, Lapoint R. Proteinase-activated receptor-2 stimulates prostaglandin production in keratinocytes: analysis of prostaglandin receptors on human melanocytes and effects of PGE2 and PGF2alpha on melanocyte dendricity. J Invest Dermatol. 2004; 122(5):1214–1224. [PubMed: 15140225]
41. Buddenkotte J, Stroh C, Engels IH, Moormann C, Shpacovitch VM, Seeliger S, et al. Agonists of proteinase-activated receptor-2 stimulate upregulation of intercellular cell adhesion molecule-1 in primary human keratinocytes via activation of NF-kappa B. J Invest Dermatol. 2005; 124(1):38–45. [PubMed: 15654951]
42. Frateschi S, Camerer E, Crisante G, Rieser S, Membrez M, Charles RP, et al. PAR2 absence completely rescues inflammation and ichthyosis caused by altered CAP1/Prss8 expression in mouse skin. Nat Commun. 2011; 2:161. [PubMed: 21245842]
43. Lindner JR, Kahn ML, Coughlin SR, Sambrano GR, Schauble E, Bernstein D, et al. Delayed onset of inflammation in protease-activated receptor-2- deficient mice. J Immunol. 2000; 165(11):6504–6510. [PubMed: 11086091]
44. Perez-Moreno M, Davis MA, Wong E, Pasolli HA, Reynolds AB, Fuchs E. p120-catenin mediates inflammatory responses in the skin. Cell. 2006; 124(3):631–644. [PubMed: 16469707]
45. Cataisson C, Salcedo R, Hakim S, Moffitt BA, Wright L, Yi M, et al. IL-1R-MyD88 signaling in keratinocyte transformation and carcinogenesis. J Exp Med. 2012; 209(9):1689–1702. Epub 2012/08/22. [PubMed: 22908325]
46. Szabo R, Uzzun Sales K, Kosa P, Shylo NA, Godiksen S, Hansen KK, et al. Reduced prostasin (CAP1/PRSS8) activity eliminates HAI-1 and HAI-2 deficiency-associated developmental defects

by preventing matriptase activation. PLoS Genet. 2012; 8(8):e1002937. Epub 2012/09/07. [PubMed: 22952456]

47. Friis S, Sales KU, Godiksen S, Peters DE, Lin CY, Vogel LK, et al. A matriptase-prostasin reciprocal zymogen activation complex with unique features: prostasin as a non-enzymatic co-factor for matriptase activation. J Biol Chem. 2013 Epub 2013/05/16.
48. Seitz I, Hess S, Schulz H, Eckl R, Busch G, Montens HP, et al. Membrane-type serine protease-1/matriptase induces interleukin-6 and-8 in endothelial cells by activation of protease-activated receptor-2: potential implications in atherosclerosis. Arteriosclerosis, thrombosis, and vascular biology. 2007; 27(4):769–775. Epub 2007/01/27.
49. Kaufmann R, Oettel C, Horn A, Halbhuber KJ, Eitner A, Krieg R, et al. Met receptor tyrosine kinase transactivation is involved in proteinase-activated receptor-2-mediated hepatocellular carcinoma cell invasion. Carcinogenesis. 2009; 30(9):1487–1496. [PubMed: 19546160]
50. Schmidlin F, Amadesi S, Dabbagh K, Lewis DE, Knott P, Bunnett NW, et al. Protease-activated receptor 2 mediates eosinophil infiltration and hyperreactivity in allergic inflammation of the airway. J Immunol. 2002; 169(9):5315–5321. Epub 2002/10/23. [PubMed: 12391252]
51. Szabo R, Hobson JP, List K, Molinolo A, Lin CY, Bugge TH. Potent inhibition and global co-localization implicate the transmembrane Kunitz-type serine protease inhibitor hepatocyte growth factor activator inhibitor-2 in the regulation of epithelial matriptase activity. J Biol Chem. 2008; 283(43):29495–29504. [PubMed: 18713750]

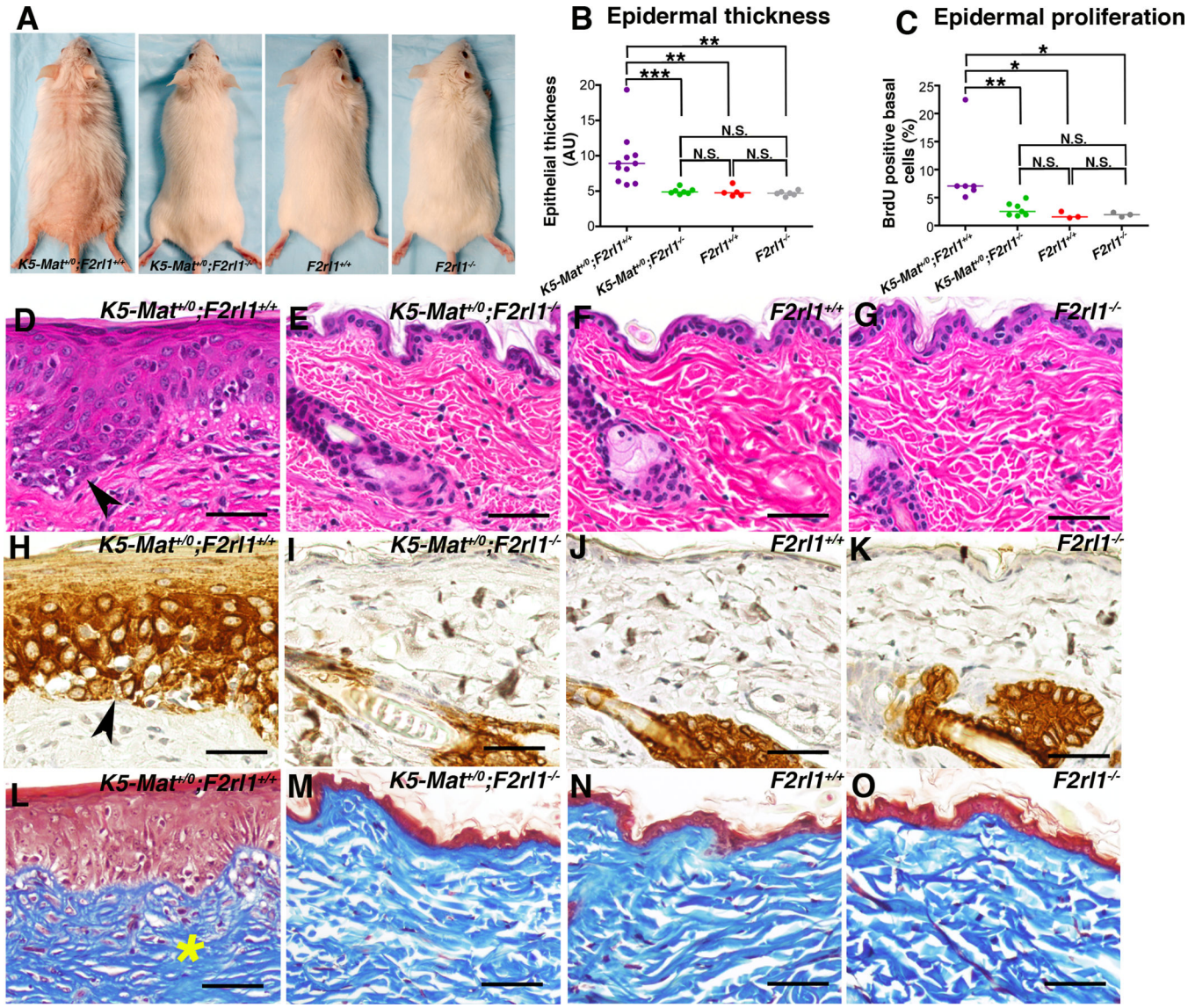

Figure 1. Matriptase-mediated pre-malignant progression of mouse squamous epithelium is PAR-2-dependent

(A). Representative examples of the outward appearance of littermate *K5-Mat*$^{+/0}$;*F2rl1*$^{+/+}$ (left panel), *K5-Mat*$^{+/0}$;*F2rl1*$^{-/-}$ (second panel from left), *F2rl1*$^{-/-}$ (second panel from right), and wildtype mice (right panel) at 52 weeks of age. Matriptase-induced alopecia and ichthyosis are prevented by genetic elimination of PAR-2. **(B).** Enumeration of epidermal thickness in littermate *K5-Mat*$^{+/0}$;*F2rl1*$^{+/+}$ (N=11, purple circles), *K5-Mat*$^{+/0}$;*F2rl1*$^{-/-}$ (N=7, green circles), wildtype (N=5, red circles), and *F2rl1*$^{-/-}$ mice (N=6, grey circles) at 52 weeks of age. *** $P < 0.0006$ (Mann-Whitney U test, two-tailed). N.S. = not significant **(C)**. Epidermal keratinocyte proliferation rates in littermate *K5-Mat*$^{+/0}$;*F2rl1*$^{+/+}$ (N=6, purple circles), *K5-Mat*$^{+/0}$;*F2rl1*$^{-/-}$ (N=7, green circles), wildtype mice (N=3, red circles), and *F2rl1*$^{-/-}$ (N=3, grey circles) at 52 weeks of age. Horizontal bars in C and B indicate median values. * $P < 0.02$, ** $P < 0.004$, *** $P < 0.0006$, N.S. = not significant (Mann-Whitney U test, two-tailed). **(D–O).** Representative histological appearance of dorsal skin of

littermate *K5-Mat*$^{+/0}$;*F2rl1*$^{+/+}$ **(D**, **H**, and **L)**, *K5-Mat*$^{+/0}$;*F2rl1*$^{-/-}$ (**E**, **I**, and **M**), wildtype mice (**F**, **J**, and **N**) and *F2rl1*$^{-/-}$ (**G**, **K**, and **O**) mice at 52 weeks of age stained with H&E (**D–G**), keratin-6 antibodies (**H–K**), and Masson's trichrome (**L–O**). Multifocal dysplasia (examples with arrowhead in **D**), interfollicular epidermal keratin-6 expression (examples with arrowhead in **H**), and dermal fibrosis (example with star in **L**) are completely prevented by genetic elimination of PAR-2. Size bars = 50 μm.

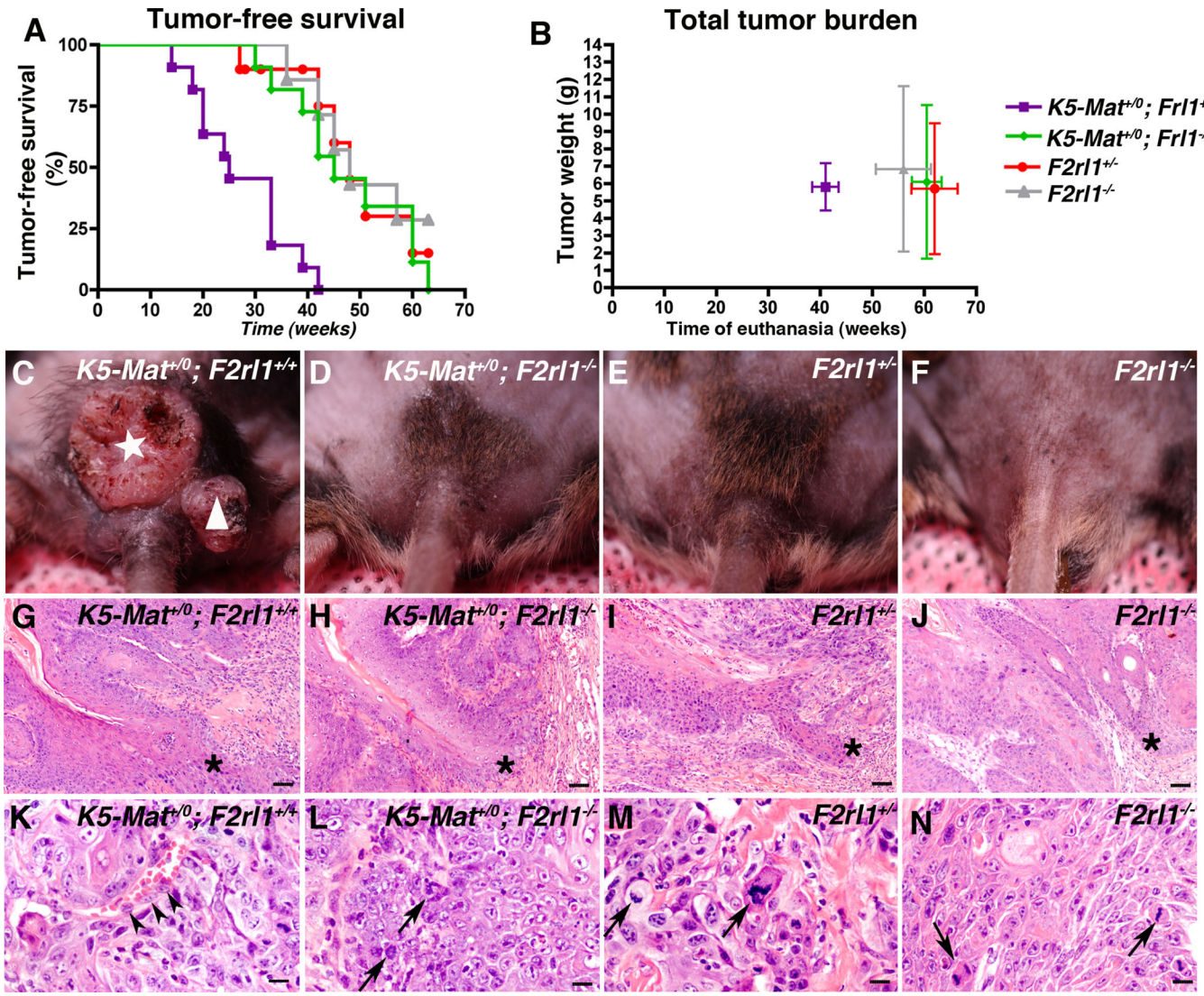

Figure 2. Dysregulated matriptase does not promote chemical carcinogenesis in the absence of PAR-2

Kaplan-Meier analysis of tumor-free survival **(A)**, and time to sacrifice and total tumor burden at sacrifice **(B)** of littermate *K5-Mat*$^{+/0}$;*F2rl1*$^{+/-}$ (N=11, purple squares), *K5-Mat*$^{+/0}$;*F2rl1*$^{-/-}$ (N=11, green diamonds), *F2rl1*$^{+/-}$ (N=10, red circles), and *F2rl1*$^{-/-}$ (N=7, grey triangles) mice. The mice were treated with DMBA every 3 weeks and were followed for up to 63 weeks. *** $P < 0.0001$, *K5-Mat*$^{+/0}$;*F2rl1*$^{+/+}$ versus other genotypes in **A** (log-rank test, two-tailed). Vertical and horizontal bars in **B** indicate standard error of the mean. **C–F**. Representative outward appearance of littermate *K5-Mat*$^{+/0}$;*F2rl1*$^{+/-}$ (left panel), *K5-Mat*$^{+/0}$;*F2rl1*$^{-/-}$ (second panel from left), *F2rl1*$^{+/-}$ (second panel from right), and *F2rl1*$^{-/-}$ (right panel) mice at 26 weeks of age. Example of carcinoma (white star) and papilloma (white triangle) in *K5-Mat*$^{+/0}$;*F2rl1*$^{+/-}$ mouse is shown. **G–N.** Representative of H&E-stained sections of squamous cell carcinoma at low (**G–J**) and high (**K–N**) magnification in a 25-week-old *K5-Mat*$^{+/0}$;*F2rl1*$^{+/-}$ (left panels) mouse, and in 45 to 55-week-old *K5-Mat*$^{+/0}$;*F2rl1*$^{-/-}$ (second panels from left), *F2rl1*$^{+/-}$ (second panels from right), and *F2rl1*$^{-/-}$

(right panels) mice showing similar histological appearance of tumors irrespective of genotype. Stars in **G–J** show examples of invasion, while arrowheads and arrows in **K–N** shows examples of cells invading vessels and atypical mitosis, respectively. Size bars. **G–J** = 100 μm. K–N = 30 μm.

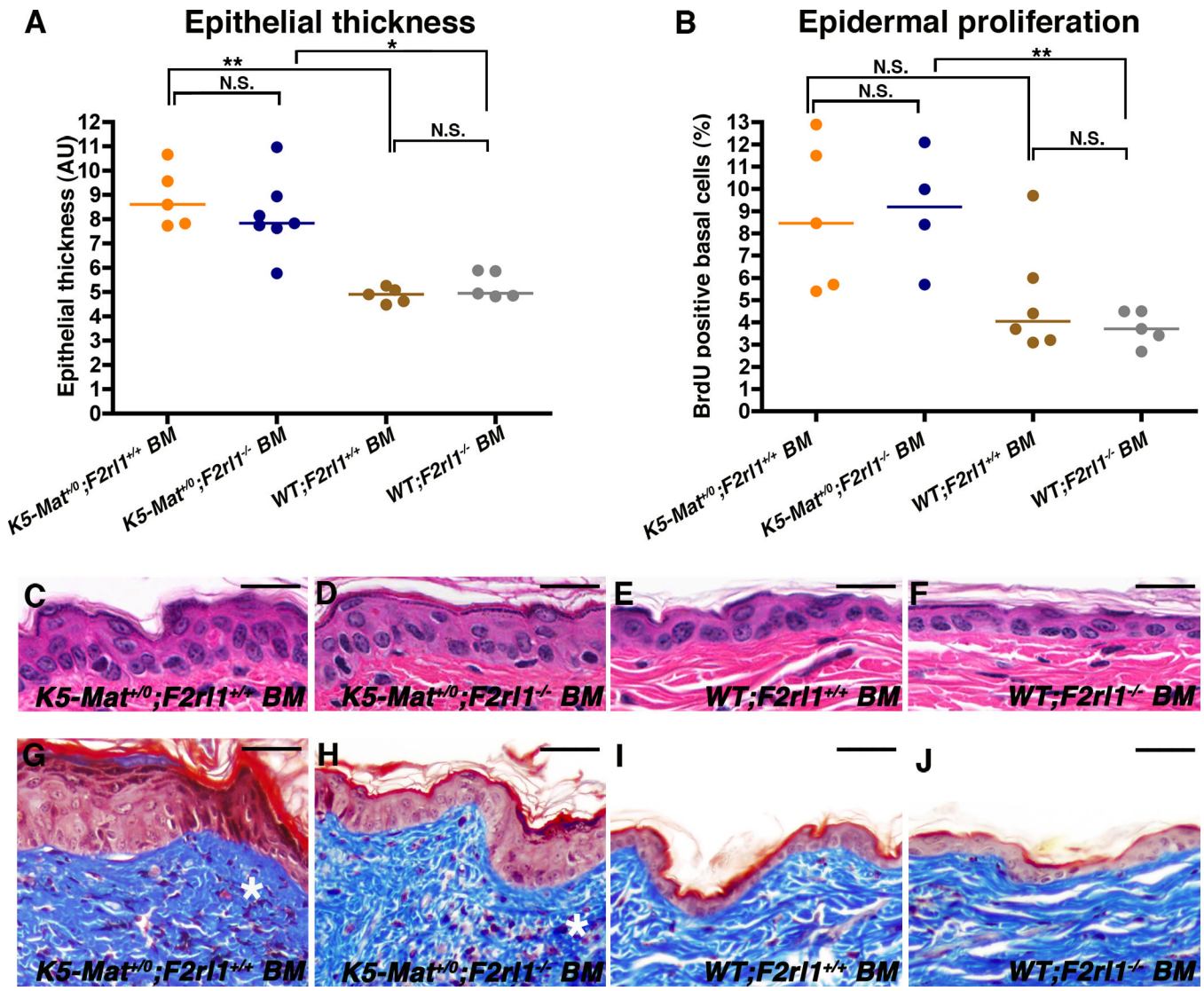

Figure 3. Hematopoietic PAR-2 is dispensable for matriptase-mediated pre-malignant progression

(A) Enumeration of epidermal thickness in 17-week-old lethally-irradiated littermate *K5-Mat*$^{+/0}$;*F2rl1*$^{+/+}$ mice (orange and blue circles) reconstituted with either *F2rl1*$^{+/+}$ (N=5, orange circles) or *F2rl1*$^{-/-}$ bone marrow (N=7, blue circles), and wildtype mice (brown and grey circles) reconstituted with *F2rl1*$^{+/+}$ (N=5, brown circles) or *F2rl1*$^{-/-}$ bone marrow (N=5, grey circles). Horizontal bars indicate median values. * $P < 0.01$ and ** $P < 0.007$, respectively, N.S. = not significant (Mann-Whitney U test, two-tailed). **(B)** Epidermal keratinocyte proliferation rates in 17-week-old lethally irradiated littermate *K5-Mat*$^{+/0}$;*F2rl1*$^{+/+}$ mice (orange and blue circles) reconstituted with either *F2rl1*$^{+/+}$ (N=5, orange circles) or *F2rl1*$^{-/-}$ bone marrow (N=4, blue circles), and wildtype mice (brown and grey circles) reconstituted with either *F2rl1*$^{+/+}$ (N=6, brown circles) or *F2rl1*$^{-/-}$ bone marrow (N=5, grey circles). Horizontal bars indicate median values. ** $P < 0.003$, N.S. = not significant ($P < 0.06$) (Student's t-test, two-tailed). **(C–J)** Representative examples of H&E (**C–F**) and Masson's trichrome (**G–J**) -stained epidermal sections from 13-weeks-old

lethally irradiated littermate *K5-Mat*$^{+/0}$;*F2rl1*$^{+/+}$ mice (**C**, **D**, **G**, and **H**) reconstituted with *F2rl1*$^{+/+}$ (**C** and **G**) or *F2rl1*$^{-/-}$ bone marrow (**D** and **H**), and wildtype mice (**E**, **F**, **I**, and **J**) reconstituted with *F2rl1*$^{+/+}$ (**E** and **I**) or *F2rl1*$^{-/-}$ (**F** and **J**) bone marrow. Stars in **G** and **H** indicate dermal fibrosis. Size bars. **C–F** = 50 μm. **G–J** = 100 μm.

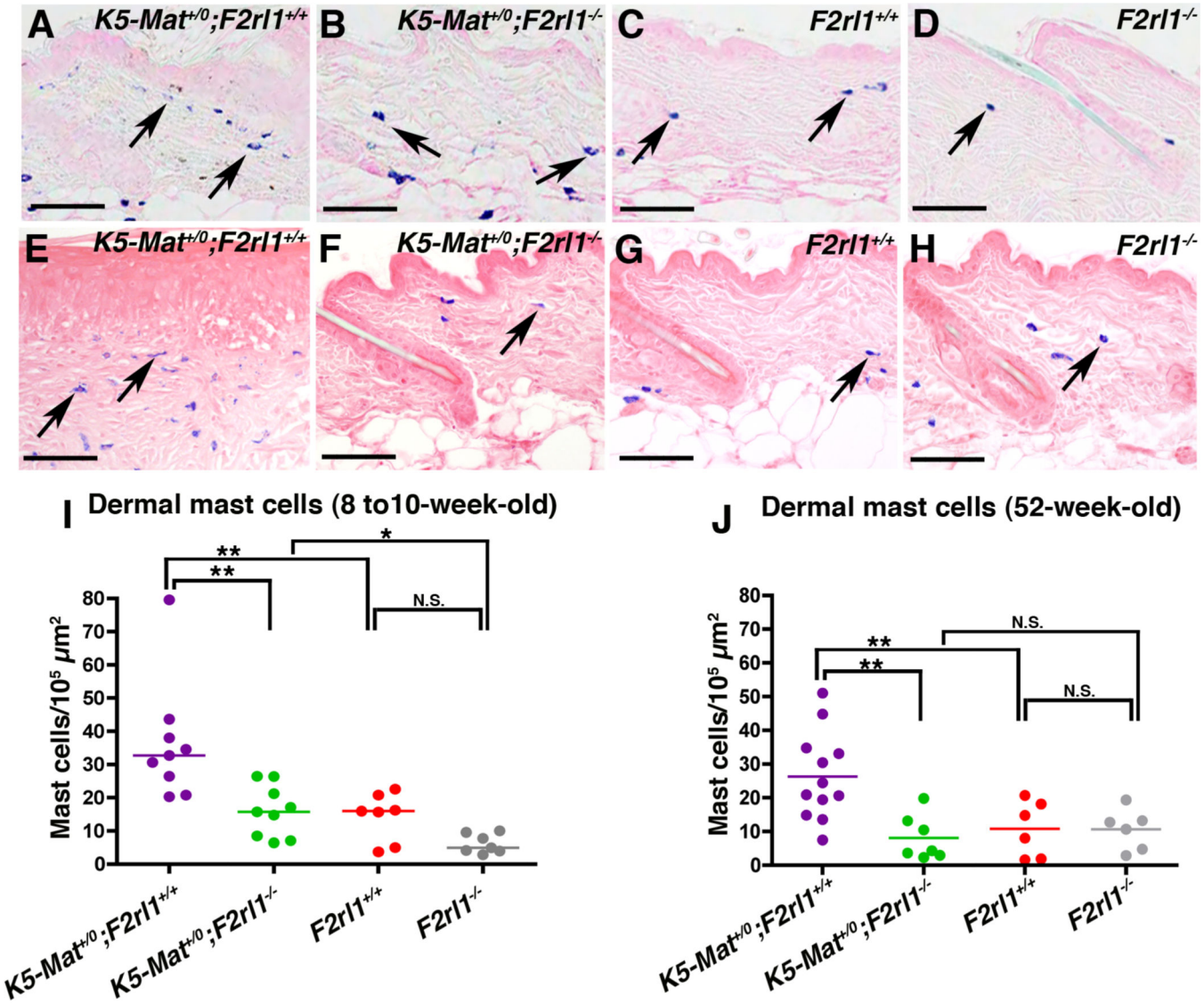

Figure 4. Matriptase-induced dermal inflammatory cell accumulation is PAR-2-dependent

A–H. Representative examples of toluidine blue-stained dorsal skin sections from 8 to 10-week-old-littermate (**A–D**) and 52-week-old littermate (**E–H**) *K5-Mat*$^{+/0}$;*F2rl1*$^{+/+}$ (left panels), *K5-Mat*$^{+/0}$;*F2rl1*$^{-/-}$ (second panels from left), *F2rl1*$^{+/+}$ (second panels from right), and *F2rl1*$^{-/-}$ (right panels) mice. Examples of dermal mast cells (blue) are indicated with arrows. Size bars = 50 µm. **(I** and **J)** Enumeration of mast cell accumulation in 8 to 10-week-old (left panel) and 52-week-old (right panel) *K5-Mat*$^{+/0}$;*F2rl1*$^{+/+}$ (N=9 to 12, purple circles), *K5-Mat*$^{+/0}$;*F2rl1*$^{-/-}$ (N=7 to 9, green circles), *F2rl1*$^{+/+}$ (N=6 to 7, red circles), and *F2rl1*$^{-/-}$ mice (N=6 to 7, grey circles). * $P < 0.01$. ** $P < 0.001$, N.S. = not significant (Mann-Whitney U test, two-tailed).

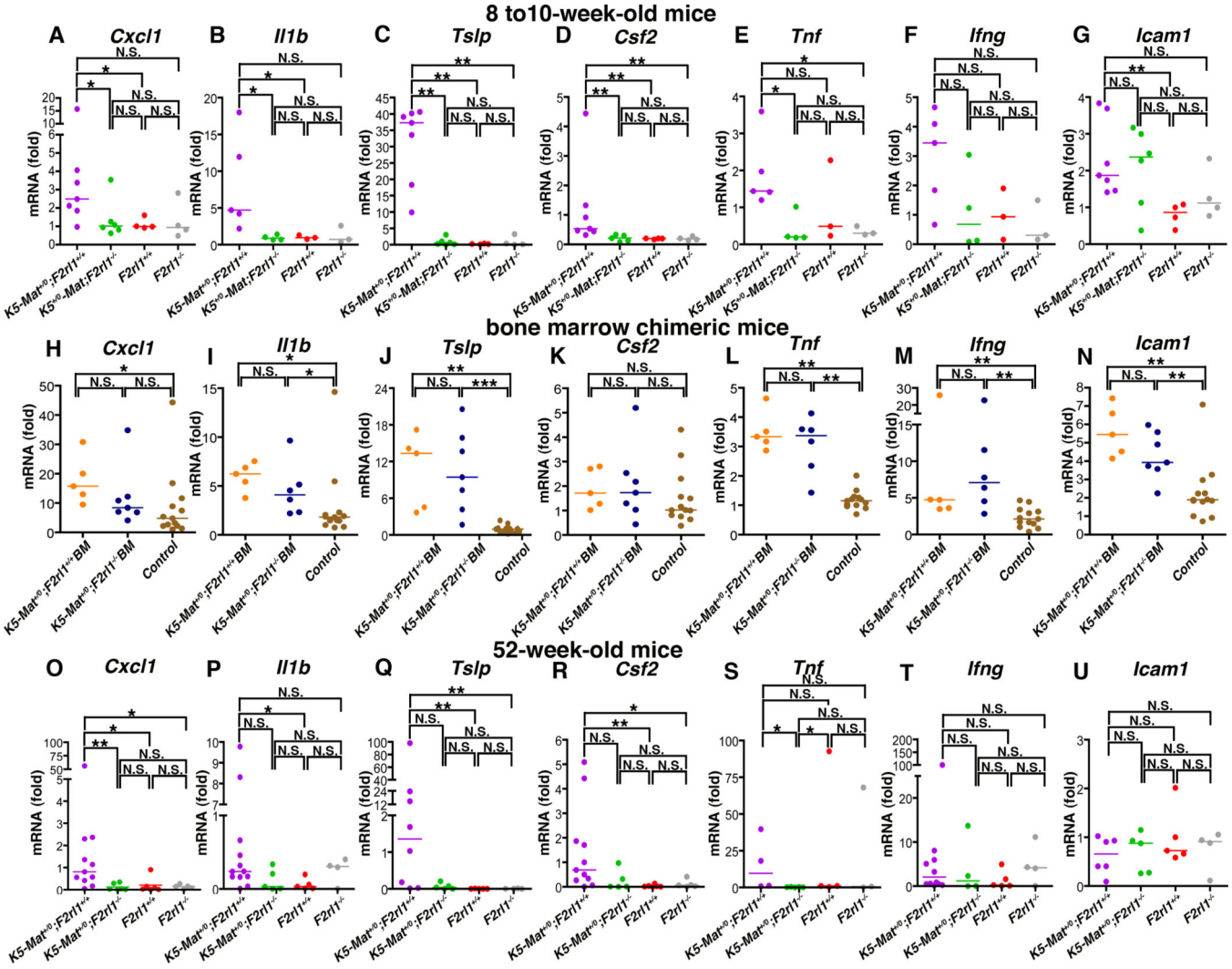

Figure 5. Dysregulated matriptase induces persistent skin inflammatory cytokine production through non-hematopoietic PAR-2

(A–G). Skin mRNA levels of *Cxcl1* **(A)**, *Il1b* **(B)**, *Tslp* **(C)**, *Csf2* **(D)**, *Tnf* (E), *Ifng* **(F)**, and *Icam1* **(G)**, in 8 to 10-week-old littermate *K5-Mat*$^{+/0}$;*F2rl1*$^{+/+}$ (N=5 to 7, purple circles), *K5-Mat*$^{+/0}$;*F2rl1*$^{-/-}$ (N=4 to 6), green circles), wildtype (N=3 to 4, red circles), and *F2rl1*$^{-/-}$ mice (N=3 to 4, grey circles). * P < 0.01, **, P < 0.001, *** P < 0.01, N.S. = not significant (Mann-Whitney U test, two-tailed). **(H–N).** Skin mRNA levels of *Cxcl1* **(H)**, *Il1b* **(I)**, *Tslp* **(J)**, *Csf2* **(K)**, *Tnf* **(L)**, *Ifng* **(M)**, and *Icam1* **(N)** in 17-week-old lethally-irradiated littermate *K5-Mat*$^{+/0}$;*F2rl1*$^{+/+}$ mice (orange and blue circles) reconstituted with *F2rl1*$^{+/+}$ (N=5, orange circles) or *F2rl1*$^{-/-}$ bone marrow (N=5 to 7, blue circles), and control (*F2rl1*$^{+/+}$ and *F2rl1*$^{-/-}$) mice (N=12 to 13, brown circles) reconstituted with either *F2rl1*$^{+/+}$ or *F2rl1*$^{-/-}$ bone marrow. Horizontal bars indicate median values. * P < 0.01, **, P < 0.001, N.S. = not significant (Mann-Whitney U test, two-tailed). **(O–U).** Skin mRNA levels of *Cxcl1* **(O)**, *Il1b* **(P)**, *Tslp* **(Q)**, *Csf2* **(R)**, *Tnf* **(S)**, *Ifng* **(T)**, and *Icam1* **(U)** in 52-week-old littermate *K5-Mat*$^{+/0}$;*F2rl1*$^{+/+}$ (N=4 to 12, purple circles), *K5-Mat*$^{+/0}$;*F2rl1*$^{-/-}$ (N=4 to 5, green circles),

wildtype (N=5, red circles), and *F2rl1*$^{-/-}$ mice (N=3 to 5, grey circles). * P < 0.01, ** P < 0.001, N.S. = not significant (Mann-Whitney U test, two-tailed).

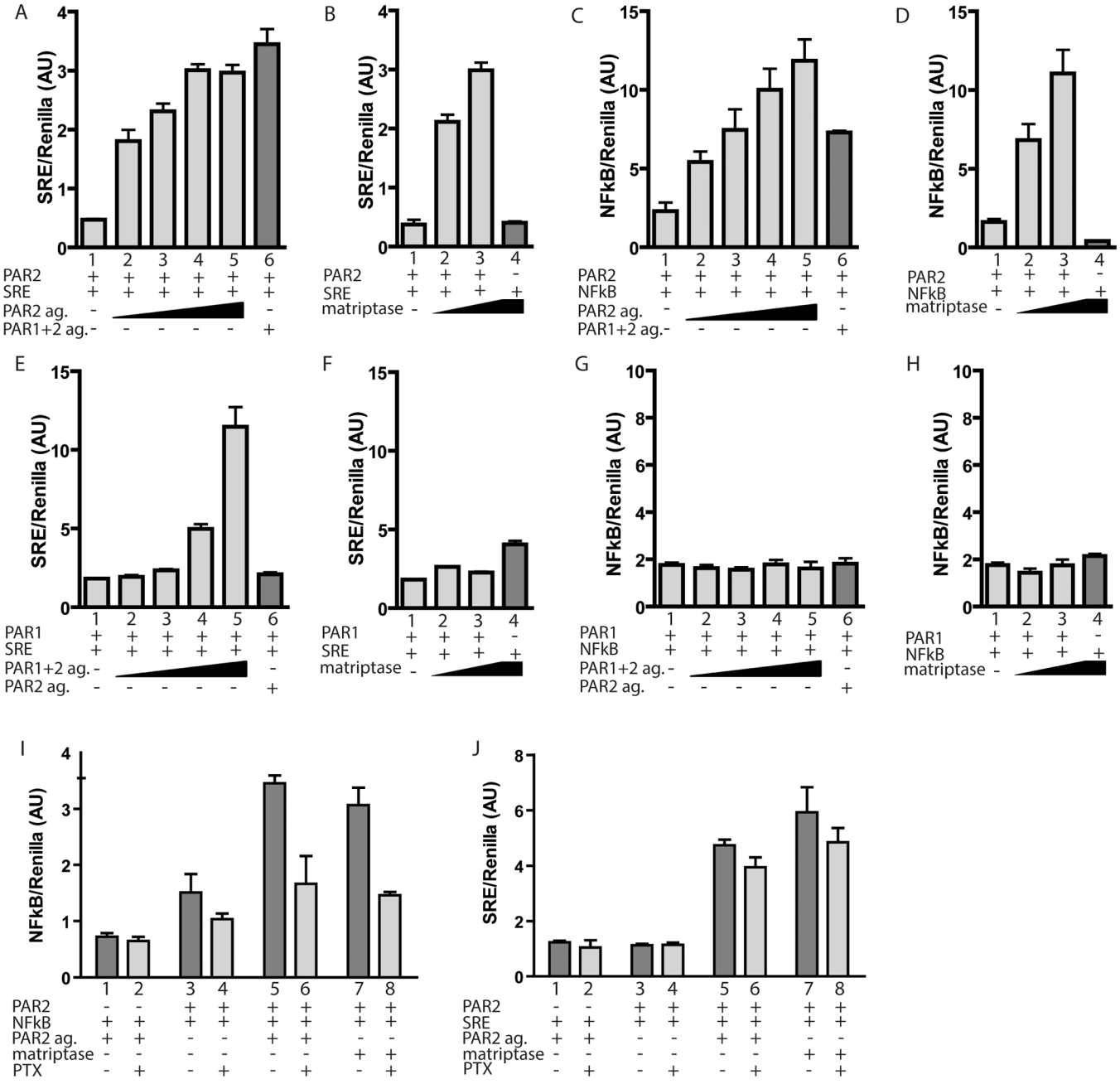

Figure 6. Matriptase can activate NFκB through PAR-2 and Gαi

(**A–H**) HEK293 cells were co-transfected with PAR-2 expression vector (PAR-2, **A–D**) or PAR-1 expression vector (PAR-1, **E–H**) or with empty expression vector and either serum response element-luciferase (SRE) (**A**, **B**, **E**, and **F**) or NFκB -luciferase reporter plasmids (NFκB) (**C**, **D**, **G**, and **H**), as indicated. The transfected cells in **A** and **C** were either treated for 6 h with the PAR-2 agonist, 2-furoyl-LIGRLO-amide (PAR-2 ag., 0.25, 1, 2.5 and 10 μM in bars 2–5 respectively) or with 10 μM dual PAR-1 and -2 agonist, TRAP-6 (lane 6). The transfected cells in **E** and **G** were either treated with TRAP-6 (0.25, 1, 2.5 and 10 μM in bars 2–5, respectively) or with 10 μM 2-furoyl-LIGRLO-amide (lane 6) for 6 h. Cells in **B**,

F, **D**, and **H** were treated with recombinant human matriptase serine protease domain for 6 h (1 or 15 nM in bars 2–4) or with vehicle (bar 4). **I** and **J**. HEK293 cells were co-transfected with empty vector (bars 1 and 2) or PAR-2 expression vector (bars 3–8) in combination with either serum response element-luciferase (**I**) or NFκB -luciferase reporter (**J**) plasmids. The transfected cells were treated overnight with vehicle (lanes 1, 3, 5, and 7) or pertussis toxin (PTX) (lanes 2, 4, 6, and 8), and then were treated with vehicle (lanes 3 and 4) or were treated with either 20 μM PAR-2 agonist (bars 1 and 2, 5 and 6) or 15 nM recombinant human matriptase (lanes 7 and 8). All cells were transfected with a pRL-Renilla luciferase reporter plasmid as an internal control for transfection efficiency. Data are shown as the mean ± standard deviation of the mean of triplicate transfections of firefly luciferase light units/Renilla luciferase light units. The data are representative of three similar experiments.